# Effects of scattering area shape on spin conductance in a four-terminal spin-Hall setup

Gunnar Thorgilsson[1] and Sigurdur I. Erlingsson[2]
[1]*Science Institute, University of Iceland, Dunhaga 3, IS-107 Reykjavik, Iceland*
[2]*School of Science and Engineering, Reykjavik University, Kringlan 1, IS-103 Reykjavik, Iceland*
(Received 8 July 2010; published 7 December 2010)

We study spin conductance in a ballistic and quasiballistic two-dimensional electron system with Rashba spin-orbit coupling. The system has a four-terminal geometry with round corners at the connection to the leads. It is found that by going from sharp corners to more round corners in the ballistic system the energy-depended spin conductance goes from being relatively flat to a curve showing a series of minima and maxima. It is also found that when changing the size of the terminal area by modifying the roundness of the terminal corners the maxima and minima in the transverse spin conductance are shifted in energy. This shift is due increased (decreased) energy for smaller (larger) terminal area. These results were also found to be reasonably stable in quasiballistic systems.

DOI: 10.1103/PhysRevB.82.245308 PACS number(s): 72.25.Dc, 71.70.Ej, 72.20.Dp, 73.23.Ad

## I. INTRODUCTION AND MOTIVATION

Spin-orbit (SO) coupling in semiconductor nanostructures has for some time been considered as one of the main candidates in controlling spin in semiconductor spintronic devices.[1–3] One of the main benefits of the SO coupling is that it can be used to manipulate electron spins in semiconductors through gate voltages instead of external magnetic fields[4] or magnetic doping.[5] SO coupling arises from relativistic effects and when combined with $\boldsymbol{k}\cdot\boldsymbol{p}$—calculation it will lead to spin-orbit terms depending on the crystal structure, i.e., the Dresselhaus SO coupling[6,7] in crystals that lack inversion symmetry. In addition, further spin-orbit contributions can occur at heterostructure interfaces. This contribution is the so-called Rashba SO coupling.[7,8] Voltages applied to local gates can change the heterostructure confining potential, thus modifying the Rashba SO coupling.[9,10] More recently, yet a new type of spin-orbit interaction has been found in symmetric two-dimensional (2D) quantum structures with two subbands: the intersubband induced spin-orbit coupling.[11,12]

In the field of spintronics the main goals is the creation and detection of spin currents. In electron-doped semiconductor structures one of the main candidates for spin-current creation is the so-called spin-Hall effect.[13] Although it has been proved that in extended 2D systems the spin-Hall effect vanishes,[14–16] this results does not hold in finite-size systems. The exception here are systems with the intersubband induced spin-orbit coupling,[11,12] which gives rise to a nonzero spin-Hall effect,[17] even for extended systems. The interplay of in-plane confinement and spin-orbit interaction leads to many interesting spin-related transport phenomena.

The Rashba SO coupling has been in recent years extensively studied both experimentally[10,18–23] and theoretically, either in two-terminal setups,[24–29] or in multiterminal setups.[27,30–34] Previous numerical studies hint that the shape of the scattering area of the system plays a vital role in the behavior of the spin current flowing through the transverse leads.[31,32]

In this work we will present calculation of spin conductance through transverse leads in a four-terminal spin-Hall setup where the shape of the scattering region is changed. Most lattice model calculations[27,30–34] used abrupt edges in the way the leads where connected to the scattering region. This abruptness leads to substantial scattering (both of charge and spin) which can suppress spin-related phenomena that one is interested in. We use smooth connection of leads to the scattering area. Since most semiconductor heterostructures are defined by gates, one would expect relatively smooth confining potentials.[35] We study the spin conductance as a function of scattering area shape and propose an explanation of the observed connection between the spin conductance and the change in size of the scattering region. We also observe that the values of spin conductance are relatively large which is due to the smooth transfer of electrons from the longitudinal leads to the transverse one.

The paper is organized as follows. In Sec. II we present the theory behind the calculations. Section III defines the parameters used in the calculations and presents the results for the ballistic system in Sec. III A and for the quasiballistic system in Sec. III B. Finally Sec. IV contains conclusions and discussion.

## II. THEORY

We are interested in a four-terminal two-dimensional electron gas (2DEG) in a semiconductor heterostructure. A schematic of the scattering region of the system can be seen in Fig. 1. The system is described by the following effective mass Hamiltonian:

$$H(x,y) = \frac{p_x^2 + p_y^2}{2m^*} + V_{\mathrm{C}}(x,y) + H_{\mathrm{R}}(x,y), \tag{1}$$

where $m^*$ is the effective electron mass. $V_{\mathrm{C}}(x,y)$ describes a hard-wall confining potential shape of the four-terminal junction with round corners. The roundness of each corner can be controlled independently by varying the radii of the circular corners, $R_{\mathrm{C1}}$ and $R_{\mathrm{C2}}$. In a region centered on the scattering area we have a SO coupling which is described by the symmetrized Rashba Hamiltonian

 

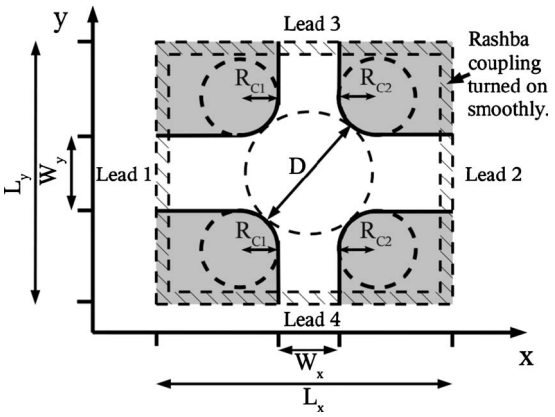


FIG. 1. Schematic picture of the four-terminal system. Sharp corners are replaced by round corners with radii $R_{C1}$ and $R_{C2}$, see Fig. 1. The whole system has a length of $L_x=102a=600$ nm and width of $L_y=L_x$. Leads 1 and 2 are the main leads into the system with a width of $W_y=41a=241$ nm while leads 3 and 4 are the transverse leads into the system with a width of $W_x=18a=106$ nm. The Rashba SO coupling is turned on smoothly on a $10a=58.8$ nm thick strip framing the system (hatched area in the figure). Inside the scattering region is shown a circle of width $D$ which we use to estimate the size of the terminal area.

$$H_{\mathrm{R}}(x,y)=\frac{1}{2\hbar}\{\alpha(x,y),(p_y\sigma_x-p_x\sigma_y)\}. \tag{2}$$

Here $\alpha(x,y)$ is the Rashba SO coupling strength which is turned on smoothly at the edges of the scattering region. Having Rashba SO coupling only in a finite area of the sample can be achieved by using metallic gate on top of the 2DEG.[36] The Hamiltonian is discretized on a square lattice using the finite-difference method, resulting in an infinitely large matrix. The corresponding matrix equation for the retarded Green's-function matrix of the system is

$$(E\mathbf{I}-\mathbf{H})\mathbf{G}^{\mathrm{r}}=\mathbf{I}. \tag{3}$$

The scattering region part of the Hamiltonian, Eq. (3), can be made finite by treating the leads as self-energies in the standard way.[37,38] The leads have no SO coupling. The finite version of the matrix equation is

$$\left(E\mathbf{I}-\mathbf{H}_{\mathrm{s}}-\sum_j \mathbf{\Sigma}_j\right)\mathbf{G}_{\mathrm{s}}^{\mathrm{r}}=\mathbf{I}. \tag{4}$$

Here the self-energy of lead $j$ is $\mathbf{\Sigma}_j$, $\mathbf{H}_{\mathrm{s}}$ is the Hamiltonian of the scattering region and $\mathbf{G}_{\mathrm{s}}^{\mathrm{r}}$ is the retarded Green's function. All the matrices are $2N_xN_y\times 2N_xN_y$ matrices. In order to save computational power only the necessary Green's-function matrix elements are calculated with the recursive Green's-function method.[38] From the Green's function both the spin conductance and spin densities can be calculated. The $z$ spin density for a bias of $eV_0$ is

$$\langle \mathbf{S}_z(\mathbf{r})\rangle=\frac{\hbar}{2}\int_{E_{\mathrm{F}}-eV_0/2}^{E_{\mathrm{F}}+eV_0/2}\frac{dE}{2\pi i}\mathrm{Tr}_{\mathrm{spin}}[\sigma_z\mathbf{G}^{<}(\mathbf{r},\mathbf{r};E)], \tag{5}$$

where $\sigma_z$ is the Pauli matrix for the $z$ direction,

$$\mathbf{G}^{<}(\mathbf{r},\mathbf{r};E)=i\left\{\mathbf{G}_{\mathrm{s}}^{\mathrm{r}}(E)\left[\sum_j f_j(E)\mathbf{\Gamma}_j(E)\right]\mathbf{G}_{\mathrm{s}}^{\mathrm{a}}(E)\right\}_{\mathbf{r},\mathbf{r}} \tag{6}$$

is the lesser Green's function,[39] $\mathbf{\Gamma}_j=-2\,\mathrm{Im}(\mathbf{\Sigma}_j)$, and $f_j(E)=1/\{\exp[\beta(E-\mu_j)]+1\}$ is the Fermi function in lead $j$ which has the chemical potential $\mu_j=E_{\mathrm{F}}+eV_j$. We define the spin-dependent conductance between the leads $q$ and $p$ as

$$G_{pq}^{\sigma\sigma'}=\frac{e^2}{h}[\mathrm{Tr}(\sigma_z\mathbf{\Gamma}_q\mathbf{G}_{\mathrm{s}}^{\mathrm{r}}\mathbf{\Gamma}_p\mathbf{G}_{\mathrm{s}}^{\mathrm{a}})]_{\sigma,\sigma'}. \tag{7}$$

Using the Landauer Büttiker formula we write the linear response of the $\sigma=\uparrow,\downarrow$ spin-depended current through lead $p$ as

$$I_p^{\sigma}=\sum_{q,\sigma'}G_{qp}^{\sigma,\sigma'}(V_p-V_q). \tag{8}$$

## III. NUMERICAL SIMULATIONS

The dimension of the scattering area is set within a $L_x\times L_y$ box-shaped area, where $L_x=L_y=600$ nm. This area is discretized on a $102\times 102$-point grid with constant mesh size $a=5.88$ nm and the effective electron mass is set as $m^*=0.0447m_{\mathrm{e}}$, which is a reasonable value for $Ga_{1-x}In_xAs$ alloys.[40] In the simulations all lengths where scaled in the mesh size $a$ and energies in the tight-binding hopping term $t=\hbar^2/2m^*a^2=24.6$ meV which results from the finite-difference discretization of the Hamiltonian in Eq. (1). Four leads connect to the system, two main leads with width $W_y=41a=241$ nm (leads 1 and 2) and two transverse leads with width $W_x=18a=106$ nm (leads 3 and 4). In the following, the energy will be scaled in the lowest transverse energy of the main leads, $E_0=0.145$ meV$=5.89\times 10^{-3}t$. Similarly we also define $E_{\mathrm{t}}=5.46E_0$ which is the lowest transverse energy of the transverse leads. The effect of Rashba SO coupling is turned on smoothly over a $10a=58.8$ nm strip at the edge of the scattering area, see the hatched area in Fig. 1, to its full strength $\alpha_0$. Between the two main leads we apply a bias $eV_0=1E_0$. This means that the chemical potentials at the leads measured from $E_{\mathrm{F}}$ will be $eV_1=eV_0/2$, $eV_2=-eV_0/2$, and $eV_3=eV_4=0$. According to Eq. (8) the spin-depended current ($\sigma=\uparrow,\downarrow$) is then

$$I_t^{\sigma}=(G_{t2}^{\sigma\sigma}+G_{t2}^{\sigma\bar{\sigma}}-G_{t1}^{\sigma\sigma}-G_{t1}^{\sigma\bar{\sigma}})\frac{V_0}{2}\quad t=3,4. \tag{9}$$

We define the spin-Hall conductance in transverse lead $t$ as

$$G_{\mathrm{sH}_t}=\frac{\hbar}{2e}\frac{I_t^{\uparrow}-I_t^{\downarrow}}{V_0}\quad t=3,4. \tag{10}$$

Note that in our scenario the total charge current through the transverse leads is always zero because of how we define the bias over the leads. Throughout the paper the full strength of the Rashba SO coupling will be set as $\alpha_0=10$ meV nm $=2at_{\mathrm{SO}}$, where $t_{\mathrm{SO}}=3.46\times 10^{-2}t$. This value of Rashba SO coupling is typical for $Ga_{1-x}In_xAs$ alloys and is also in the regime where we begin to see strong and interesting features in spin conductance through the transverse lead.

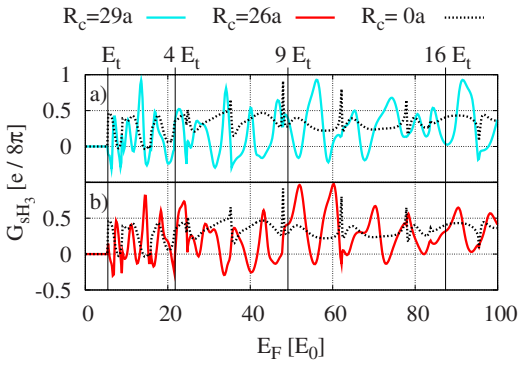


FIG. 2. (Color online) Spin conductance through lead 3 plotted as a function of Fermi energy. (a) correspond to the four-terminal shape where $R_C=29a$ and (b) correspond to $R_C=26a$. In both figures the spin conductance through a $R_C=0a$ system (sharp corners) is plotted for comparison. The bottom of the energy bands of transverse leads (with energy scaled in $E_t$) have been marked onto the figure. Note that the $y$ scale is unique for each of the figures.

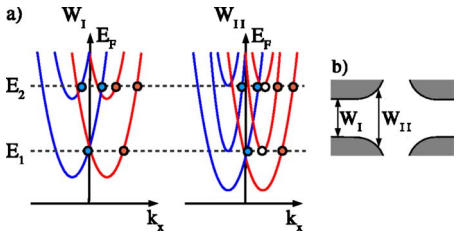


FIG. 3. (Color online) Schematic picture showing the effective shift in the transverse Rasbha energy bands, see (a), when the system gets wider, see (b). In (a) the left energy bands corresponds to the system where the width is $W_I$ and the right energy bands correspond to the system where the width is $W_{II}$. Here $k_x$ is the longitudinal $k$ vector of the electrons. The red lines (shifted to the right) correspond to spin-up states and the blue lines (shifted to the left) to spin-down states. At Fermi energies $E_1$ and $E_2$ we get additional states with low longitudinal velocities ($v_x \approx 0$), marked with white dots, in addition to the states with positive velocities, marked with red and blue dots. In the terminal area the electrons from the original positive longitudinal velocity states can scatter into these newly open states.

### A. Ballistic system

We will start by showing the spin-Hall conductance through the transverse leads in a clean system. In Fig. 2 the spin-Hall conductance through lead 3, $G_{sH_3}$, is plotted as a function of Fermi energy $E_F$ for three types of shapes. Figure 2(a) corresponds to shape with $R_C=29a$, Fig. 2(b) to $R_C=26a$. In both figures the spin conductance for a sharp corner system ($R_C=0a$) is plotted for comparison. Here we use $R_C=R_{C1}=R_{C2}$ when all the corners have the same curvature.

In Figs. 2(a) and 2(b), we see that the spin conductance curves corresponding to the round corner systems ($R_C=29a$ and $R_C=26a$) are rich in minima and maxima. These extrema are most likely related to the resonance states in the scattering area which we will discuss below.

The resonance states form when the leads get adiabatically larger which results in a downward shift in the transverse energy bands of the leads,[41] see Fig. 3. This causes new states to become available at the Fermi energy which have very low longitudinal velocity ($v_x \approx 0$). Near the transverse leads the adiabatic approximation ceases to apply and the electron scatter in to different states, including the newly opened low longitudinal velocity states which give rise to conductance extrema in the transverse leads.

The sharp corner $G_{sH_3}$ curve, shown both in Figs. 2(a) and 2(b), behaves differently. At high enough energies ($E_F > 30E_0$) the curve changes slowly with energy and has no significant resonance peaks, apart from isolated peaks due to divergence in the density of states at energies corresponding to the band bottom in the longitudinal leads. The observed behavior of the sharp corner $G_{sH_3}$ is due to the strong scattering by the sharp corners. An electron coming in from the left, with a definite $k$ value, gets scattered into all possible states, with the same energy, when it enters the scattering region. For higher energies these states are very many, all corresponding to different effective magnetic fields which tend to average out the spin signal. Note that for low energies we still see peaks and minima since only a few $k$ states are available at such low energies.

Comparing the round corner curves in Figs. 2(a) and 2(b) we see that the extrema at $E_F=56E_0$ in Fig. 2(a) has shifted to $E_F=60E_0$ in Fig. 2(b). Other extrema in $G_{sH_3}$ seem also to have been shifted by the change in corner radius $R_C$. To explore in more detail this shift of extrema in $G_{sH_3}$ with change in curvature we make a surface plot of the spin-Hall conductance through lead 3, $G_{sH_3}$, as a function of Fermi energy varied from $0E_0$ to $100E_0$ and $R_C$ varied from $0a$ (sharp corners) to $30a$ with interval of $1a$. The result can be seen in Fig. 4(a). There we see that for low corner curvatures ($R_C \lesssim 10a$) the spin conductance becomes smeared out as was discussed above.

For higher corner curvatures ($R_C \gtrsim 10a$) we get a spin conductance curve which shows a series of minima and maxima. Extrema in $G_{sH_3}$ also begin to shift in energy with increasing corner curvature. For smoother corners the transport gets more adiabatic and the extrema in $G_{sH_3}$ will be more influenced by geometric resonances, i.e., changes in shape will be adiabatically translated into a shift in the energy bands that will affect the transport. Changing the curvature of the scattering region effectively changes its area. For smooth enough corners, the shape of the system is not affected by changing the curvature, only its size, which results in a universal shift of all bands in the scattering area. This does not apply to the sharp corners, where a small change in curvature can results in great change in scattering properties.

The effective diameter of the scattering region is $D=(\sqrt{2}-1)(R_{C1}+R_{C2})+\sqrt{W_x^2+W_y^2}$, see Fig. 1. The energy shift of a given $G_{sH_3}$ extrema will be $E_C \propto D^{-2}$. The prefactor is not known but this does not matter as we will show here below. We can pick a reference energy $E_{C_0}$, with reference size $D_0=(\sqrt{2}-1)(R_{C1_0}+R_{C2_0})+\sqrt{W_A^2+W_B^2}$, on the same extrema in $G_{sH_3}$. By dividing $E_C$ with this reference energy $E_{C_0}$ we get rid of the unknown prefactor in $E_C$ and obtain

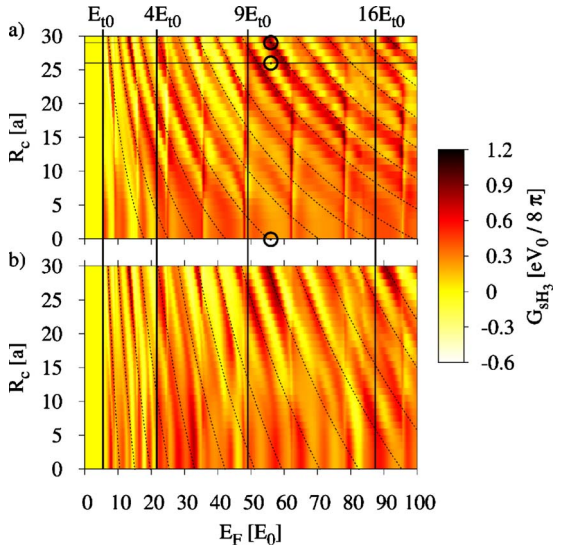


FIG. 4. (Color online) Spin conductance through lead 3 plotted as a function of radii of the corners and Fermi energy. In (a) all corners are equally varied while in (b) two corners are varied equally, the $R_{C1}$ corners, and two corners are kept fixed, $R_{C2}=30a$. The black dashed lines show the shift of $G_{sH}$ maxima in energy according to Eq. (11). The horizontal black lines mark where the spin conductance through lead 3 in Figs. 2(a) and 2(b) lie and the black circles show the ($R_C$, $E_F$) coordinates of the spin densities shown in Fig. 5. The vertical black lines mark the bottom of the transverse energy bands scaled in $E_t=5.46E_0$.

$$E_C = \left[\frac{(\sqrt{2}-1)(R_{C1_0}+R_{C2_0})+\sqrt{W_x^2+W_y^2}}{(\sqrt{2}-1)(R_{C1}+R_{C2})+\sqrt{W_x^2+W_y^2}}\right]^2 E_{C_0}, \quad (11)$$

which describes the shift of the energy levels in the scattering area as a function of the shape of the scattering area.

In Fig. 4(a) we have plotted curves, shown with black dashed lines, with reference points at $R_{C_0}=R_{C1_0}=R_{C2_0}=30a$ on all the spin conductance maxima. As can be seen for $R_C \gtrsim 10a$ the shift of the maxima curves fits well to the shift that we expect for adiabatic change in size of the scattering area. For $R_C \lesssim 10a$ scattering from the corners gets more dominating, which is to be expected since the system is out the adiabatic regime and the sensitivity to the corners takes over.

A shape where we keep $R_{C2}=30a$ fixed and only vary $R_{C1}$ was also examined, see Fig. 4(b). Here we also plot curves based on Eq. (11), shown with black dashed lines, with reference points at $R_{C1}=30a$ on all the maxima curves. We notice that the for low $R_{C1}$ corner curvatures, $R_{C1} \lesssim 10a$, we get somewhat more structure than for than for low $R_C$ in the equal corner shape. This is due to that only two corners are contributing to the sharp corner scattering. We also notice that for $R_{C1} \gtrsim 10a$ the shift in spin conductance maxima follows the expected shift calculated from Eq. (11).

To examine the effect of corner curvature better we also plot the density of the $z$ spin component in the scattering region for three types of all equal corner shape $R_C=29a$, see Fig. 5(a), $R_C=29a$, see Fig. 5(b), and $R_C=0a$, see Fig. 5(c). For all three types we set the bias as $eV_0=1E_0$ and temperature at $T=1$ K.

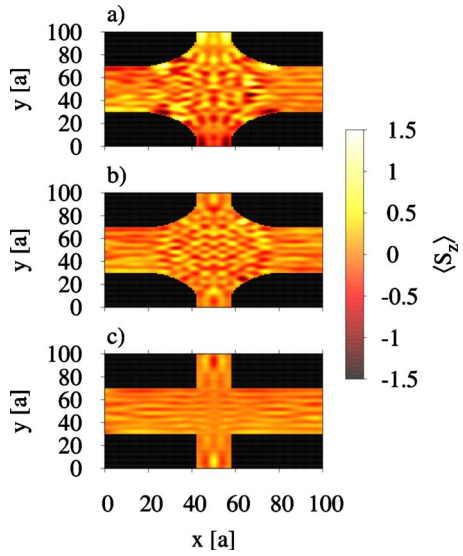


FIG. 5. (Color online) Density of the spin $z$ component in the ballistic system at $E_F=56E_0$ for three different geometries. The shape in (a) has $R_C=29a$, the shape in (b) has $R_C=26a$, and the shape in (c) has $R_C=0a$ (sharp corners). These ($E_F$,$R_C$) values correspond to the spin-Hall values marked with black circles in Fig. 4(a).

In Fig. 5(a) we have stronger spin densities along the corner edges and within the transverse leads than in Fig. 5(b). Also the spin densities averaged over the transverse leads in Fig. 5(b) is lower compared to equivalent averaging in Fig. 5(a). These densities correspond to spin conductance strength marked with black circles in Fig. 4(a) and as expected the more positive spin conductance yields more positive spin density averaged over the transverse leads. For comparison we also include spin density in the sharp corner system, see Fig. 5(c). We see that the spin density in the sharp corner system is more smeared out than in the round corner systems, as could be expected in light of previous discussion about the sharp corner system. Note though that these spin densities seen in Fig. 5 are not large, only up to $\approx 1.3\times 10^{-6}\hbar/2$ nm$^{-2}$.

The results presented in this section suggest that polarization of the spin current through the transverse leads can be effectively controlled by tuning the curvature of the corners in the scattering area. This could be realized by using, e.g., finger gates.[42]

### B. Quasiballistic system

To test how robust the $G_{sH}$ extrema are, we add impurity effects to our model. Two different methods of including impurity effects were studied. The first method which we will consider involves adding a few randomly distributed Gaussian-shaped impurities to the sample. The second method which we considered is the Anderson impurity method which has already been extensively used for similar simulations.[27–30,43,44]

#### *1. Static impurities*

Phenomena such as crystal defects can introduce extra potential bumps in the otherwise uniform potential back-

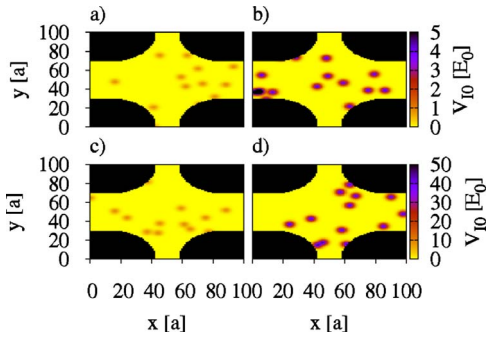


FIG. 6. (Color online) Scattering shape using $R_C=29a$ corner radii and with $N_I=20$ static impurities added on random locations in the whole box of the scattering area. All impurities are set to have range $\Gamma_I=2a$, and the impurity strength is set at $V_{I_0}=1E_0$ for impurities in (a), $V_{I_0}=5E_0$ for impurities in (b), $V_{I_0}=10E_0$ for impurities in (c), and $V_{I_0}=50E_0$ for impurities in (d).

ground. These bumps can be described as static Gaussian-shaped impurities in the scattering region which we add randomly to our scattering region via the term

$$V_I(x,y) = V_{I_0}\sum_{i=1}^{N_I} \exp\left[-\frac{(x_i-x)^2+(y_i-y)^2}{2\Gamma_I^2}\right], \qquad (12)$$

which is added to the Hamiltonian in Eq. (1). Here $V_{I_0}$ is the potential height of the potential bump, $N_I$ is the number of impurities, $(x_i,y_i)$ the center point of each impurity, and $\Gamma_I$ impurity range. We would expect the number of these impurities to be just a few percent of the number of donors. We choose 2% which corresponds to roughly $N_I=20$ Gaussian impurities in an $600\times600$ nm$^2$ area and a delta donor density of $\approx3\times10^{11}$ cm$^{-2}$. We are interested in seeing how strong these Gaussian-shaped impurities must be to have significant effect on the spin-Hall conductance. To accomplish this four cases of impurity strength were studied: $V_{I_0}=1E_0$, $V_{I_0}=5E_0$, $V_{I_0}=10E_0$, and $V_{I_0}=50E_0$, see Fig. 6. These values of impurity strength are roughly the same order of magnitude as a screened and unscreened point charge 17 nm away from

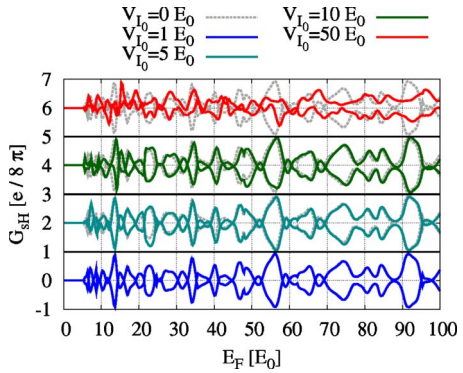


FIG. 7. (Color online) The spin conductance through lead 3 and 4 as a function of energy for the cases shown in Fig. 6 compared to the spin conductance of the clean system, see Fig. 2(a). Note that the $G_{sH}$ scale is shifted incrementally for each $V_{I_0}$ curve from the $V_{I_0}=1E_0$ curve.

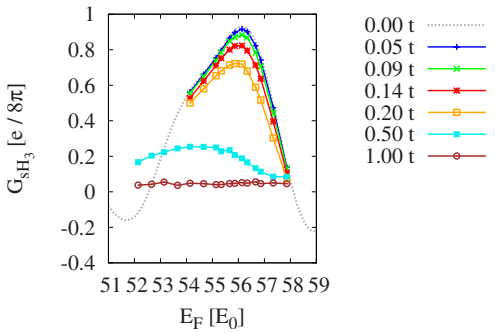


FIG. 8. (Color online) The spin conductance through lead 3 as a function of Fermi energy for a range of disorder strengths $U$. To compare we also plot he spin conductance of the ballistic system which we mark with $U=0t$. These results have been averaged over 1000 runs and the disorder strength is scaled in the tight-binding hopping term $t=171E_0$.

a 2DEG in Ga[Al]As heterostructure.[35] The effect these impurities have on the spin-Hall conductance in leads 3 and 4 can be seen in Fig. 7. There we see that up to impurity strength $V_{I_0}=10E_0$ the spin conductance is rather stable and that spin conductance through lead 3 and 4 is symmetric around zero.

### 2. *Anderson-type impurities*

The Anderson impurity potential adds to each point in the scattering area a random value of potential energy in the range $[-U/2,U/2]$, where $U$ describes the disorder strength. To study the effect of the Anderson-type impurities on $G_{sH}$ we focus on an extrema in $G_{sH_3}$ at $E_F=56E_0$ for a $R_C=29a$ scattering shape, see Fig. 2(a). In Fig. 8 the spin-Hall conductance is plotted for impurity strength ranging from $U=0.05t$ to $U=1.0t$. Each data point is averaged over 1000 impurity configurations. For comparison we include the result for the ballistic system, seen also in Fig. 2(a). In Fig. 8 we see that the structure of the spin conductance is stable up to $U=0.2t=34.2E_0$ although its amplitude diminishes and the structure shifts with increasing disorder strength. For $U=0.5t=85.5E_0$ the spin conductance seems to be disappearing as has been shown for such large disorder values.[34]

These results can be compared with the mean-free path $l$ which in two-dimensional systems is given by[44]

$$l = \frac{6\lambda_F^3}{\pi^3 a^2}\left(\frac{E_F}{U}\right)^2 = 48\frac{\sqrt{E_F}}{U^2}t^{3/2}a, \qquad (13)$$

where $\lambda_F$ is the Fermi wavelength. We see, e.g., for systems with $E_F=56E_0$ and impurity strength $U=0.05t$ ($U=0.20t$) that the mean-free path is $l=65$ $\mu$m($l=4$ $\mu$m) which is large compared to the system size, $L=600$ nm. This corresponds to systems in the quasiballistic regime. On the other hand for impurity strength $U=0.50t$ the mean-free path is $l=647$ nm which is comparable to the system size. For this value of $U$, or larger, the system is entering the diffusive regime.

## IV. CONCLUSIONS AND DISCUSSION

In this paper the effect of scattering area shape on spin conductance in a four-terminal 2DEG structure with Rashba SO coupling is studied numerically. The change in the scattering region was implemented by modifying the curvature of the corners between different leads. Both the ballistic regime and the quasiballistic regime were considered. It is found that above a certain curvature the spin conductance, $G_{sH}$, shows a series of minima and maxima, as a function of energy. These minima and maxima are shifted in energy with increasing curvature. We propose a relation between this shift of the extrema and the change in the size of the scattering area when the curvature is increased. This is due to the increased energy for smaller scattering areas and describes the observed shift of the extrema reasonably well. With this relation the polarization of the spin current through the transverse leads could effectively be controlled by tuning the curvature of the corners in the scattering area.

In addition, we have also test the robustness of the spin conductance extrema by adding impurities to the scattering area. Static and Anderson-type impurities were considered. The amplitude of the spin conductance extrema are suppressed with increasing impurity strength but the structure is shown to be stable under reasonable values of impurity strength, i.e., when the system is quasiballistic.

## ACKNOWLEDGMENTS

We gratefully acknowledge helpful discussions with Mathias Dückheim and Andrei Manolescu. This work was supported by the Icelandic Science and Technology Research Program for Postgenomic Biomedicine, Nanoscience and Nanotechnology, the Icelandic Research Fund, and the Research Fund of the University of Iceland.

[1] S. A. Wolf, D. D. Awschalom, R. A. Buhrman, J. M. Daughton, S. von Molnar, M. L. Roukes, A. Y. Chtchelkanova, and D. M. Treger, Science **294**, 1488 (2001).
[2] D. Awschalom, D. Loss, and N. Samarth, *Semiconductor Spintronics and Quantum Computation* (Springer, New York, 2002).
[3] D. D. Awschalom and M. E. Flatte, Nat. Phys. **3**, 153 (2007).
[4] G. A. Prinz, Science **282**, 1660 (1998).
[5] T. Dietl, *Materials, Properties and Preparation*, Handbook on Semiconductors Vol. 3B (North-Holland, Amsterdam, 1994).
[6] G. Dresselhaus, Phys. Rev. **100**, 580 (1955).
[7] R. Winkler, *Spin-orbit Coupling Effects in Two-Dimensional Electron and Hole Systems* (Springer, Berlin, 2010).
[8] E. I. Rashba, Fiz. Tverd. Tela (Leningrad) **2**, 1224 (1960) [Sov. Phys. Solid State **2**, 1109 (1960).]
[9] J. Nitta, T. Akazaki, H. Takayanagi, and T. Enoki, Phys. Rev. Lett. **78**, 1335 (1997).
[10] T. Schapers, V. A. Guzenko, A. Bringer, M. Akabori, M. Hagedorn, and H. Hardtdegen, Semicond. Sci. Technol. **24**, 064001 (2009).
[11] E. Bernardes, J. Schliemann, M. Lee, J. C. Egues, and D. Loss, Phys. Rev. Lett. **99**, 076603 (2007).
[12] R. S. Calsaverini, E. Bernardes, J. C. Egues, and D. Loss, Phys. Rev. B **78**, 155313 (2008).
[13] J. Sinova, D. Culcer, Q. Niu, N. A. Sinitsyn, T. Jungwirth, and A. H. MacDonald, Phys. Rev. Lett. **92**, 126603 (2004).
[14] J.-i. Inoue, G. E. W. Bauer, and L. W. Molenkamp, Phys. Rev. B **70**, 041303 (2004).
[15] O. Chalaev and D. Loss, Phys. Rev. B **71**, 245318 (2005).
[16] S. I. Erlingsson, J. Schliemann, and D. Loss, Phys. Rev. B **71**, 035319 (2005).
[17] M. Lee, M. O. Hachiya, E. Bernardes, J. C. Egues, and D. Loss, Phys. Rev. B **80**, 155314 (2009).
[18] J. B. Miller, D. M. Zumbühl, C. M. Marcus, Y. B. Lyanda-Geller, D. Goldhaber-Gordon, K. Campman, and A. C. Gossard, Phys. Rev. Lett. **90**, 076807 (2003).
[19] T. Schäpers, J. Knobbe, and V. A. Guzenko, Phys. Rev. B **69**, 235323 (2004).
[20] Y. K. Kato, R. C. Myers, A. C. Gossard, and D. D. Awschalom, Science **306**, 1910 (2004).
[21] V. Sih, R. C. Myers, Y. K. Kato, W. H. Lau, A. C. Gossard, and D. D. Awschalom, Nat. Phys. **1**, 31 (2005).
[22] V. Sih, W. H. Lau, R. C. Myers, V. R. Horowitz, A. C. Gossard, and D. D. Awschalom, Phys. Rev. Lett. **97**, 096605 (2006).
[23] P. Debray, S. M. S. Rahman, J. Wan, R. Newrock, M. Cahay, A. T. Ngo, S. E. Ulloa, S. Herbert, M. Muhammad, and M. Johnson, Nat. Nanotechnol. **4**, 759 (2009).
[24] A. Reynoso, G. Usaj, and C. A. Balseiro, Phys. Rev. B **73**, 115342 (2006).
[25] L. Zhang, P. Brusheim, and H. Q. Xu, Phys. Rev. B **72**, 045347 (2005).
[26] B. K. Nikolić and S. Souma, Phys. Rev. B **71**, 195328 (2005).
[27] B. K. Nikolić, S. Souma, L. P. Zârbo, and J. Sinova, Phys. Rev. Lett. **95**, 046601 (2005).
[28] B. K. Nikolić, L. P. Zârbo, and S. Welack, Phys. Rev. B **72**, 075335 (2005).
[29] M. Duckheim, D. Loss, M. Scheid, K. Richter, I. Adagideli, and P. Jacquod, Phys. Rev. B **81**, 085303 (2010).
[30] M. S. Garelli and J. Schliemann, Phys. Rev. B **80**, 155321 (2009).
[31] Y. Xing, Q.-f. Sun, and J. Wang, Phys. Rev. B **73**, 205339 (2006).
[32] T. Yokoyama and M. Eto, Phys. Rev. B **80**, 125311 (2009).
[33] M. Yamamoto, T. Ohtsuki, and B. Kramer, Phys. Rev. B **72**, 115321 (2005).
[34] B. K. Nikolić, L. P. Zârbo, and S. Souma, Phys. Rev. B **72**, 075361 (2005).
[35] T. Ihn, *Semiconductor Nanostructures: Quantum States and Electronic Transport* (Oxford University Press, New York, 2010).
[36] G. Engels, J. Lange, T. Schäpers, and H. Lüth, Phys. Rev. B **55**, R1958 (1997).
[37] S. Datta, *Electronic Transport in Mesoscopic Systems* (Cambridge University Press, Cambridge, England, 1995).
[38] D. K. Ferry and S. M. Goodnick, *Transport in Nanostructures* (Cambridge University Press, Cambridge, England, 1997).
[39] H. J. W. Haug and A.-P. Jauho, *Quantum Kinetics in Transport*

*and Optics of Semiconductors: Second, Substantially*, rev. ed. (Springer, Berlin, 2008).

[40] M. Levinshtein, S. Rumyantsev, and M. Shur, *Handbook Series on Semiconductor Parameters* (World Scientific, Singapore, 1996), Vol. 2.

[41] H. U. Baranger, D. P. DiVincenzo, R. A. Jalabert, and A. D. Stone, Phys. Rev. B **44**, 10637 (1991).

[42] C.-T. Liang, O. A. Tkachenko, V. A. Tkachenko, D. G. Baksheyev, M. Y. Simmons, D. A. Ritchie, and M. Pepper, Phys. Rev. B **70**, 195324 (2004).

[43] M. P. Anantram and T. R. Govindan, Phys. Rev. B **58**, 4882 (1998).

[44] A. Grincwajg, G. Edwards, and D. K. Ferry, J. Phys.: Condens. Matter **9**, 673 (1997).